7-28-2020

Reshaping of Truncated Pd Nanocubes: Energetic and Kinetic Analysis Integrating Transmission Electron Microscopy with Atomistic-Level and Coarse-Grained Modeling

King C. Lai
Iowa State University and Ames Laboratory, kclai@iastate.edu

Minda Chen
Iowa State University, mchen@iastate.edu

Benjamin Williams
Boston College

Yong Han
Iowa State University, y27h@iastate.edu

Chia-Kuang Tsung
Boston College

See next page for additional authors

Reshaping of Truncated Pd Nanocubes: Energetic and Kinetic Analysis Integrating Transmission Electron Microscopy with Atomistic-Level and Coarse-Grained Modeling

Abstract

Stability against reshaping of metallic fcc nanocrystals synthesized with tailored far-from-equilibrium shapes is key to maintaining optimal properties for applications such as catalysis. Yet Arrhenius analysis of experimental reshaping kinetics, and appropriate theory and simulation, is lacking. Thus, we use TEM to monitor the reshaping of Pd nanocubes of ∼25 nm side length between 410 °C (over ∼4.5 h) and 440 °C (over ∼0.25 h), extracting a high effective energy barrier of Eeff ≈ 4.6 eV. We also provide an analytic determination of the energy variation along the optimal pathway for reshaping that involves transfer of atoms across the nanocube surface from edges or corners to form new layers on side {100} facets. The effective barrier from this analysis is shown to increase strongly with the degree of truncation of edges and corners in the synthesized nanocube. Theory matches experiment for the appropriate degree of truncation. In addition, we perform simulations of a stochastic atomistic-level model incorporating a realistic description of diffusive hopping for undercoordinated surface atoms, thereby providing a visualization of the initial reshaping process.

Keywords

truncated Pd nanocubes, reshaping energetics and kinetics, transmission electron microscopy, atomistic and coarse-grained modeling, kinetic Monte Carlo simulation

Disciplines

Engineering Physics | Materials Chemistry | Nanoscience and Nanotechnology

Authors

King C. Lai, Minda Chen, Benjamin Williams, Yong Han, Chia-Kuang Tsung, Wenyu Huang, and James W. Evans

Reshaping of Truncated Pd Nanocubes: Energetic and Kinetic Analysis integrating TEM, DFT, KMC, and Analytic Theory

King C. Lai,[1,2] Minda Chen,[3] Benjamin P. Williams,[4] Yong Han,[1,2] Chia-Kuang Tsung,[4] Wenyu Huang,[3] and James W. Evans[1,2]

[1]Ames Laboratory – USDOE, Division of Chemical & Biological Sciences, Iowa State University, Ames, Iowa 50011
[2]Department of Physics & Astronomy, Iowa State University, Ames, Iowa 50011
[3]Department of Chemistry, Iowa State University, Ames Iowa 50011
[4]Department of Chemistry, Merkert Chemistry Center, Boston College, 2609 Beacon Street, Chestnut Hill, Massachusetts 02467

ABSTRACT

Stability against reshaping of metallic fcc nanocrystals synthesized with tailored far-from-equilibrium shapes is key to maintaining optimal properties for applications such as catalysis. Yet Arrhenius analysis of experimental reshaping kinetics, and appropriate theory and simulation, is lacking. Thus, we use TEM to monitor the reshaping of Pd nanocubes of ~25 nm side length between 410 °C (over ~4.5 hr) and 440 °C (over ~0.25 hr) extracting a high effective energy barrier of $E_{\text{eff}} \approx 4.6$ eV. We also provide an analytic determination of the energy variation along the minimum energy path for reshaping which involves transfer of atoms across the nanocube surface from edges or corners to form new layers on side {100} facets. The effective barrier from this analysis is shown to increase strongly with the degree of truncation of edges and corners in the synthesized nanocube. Theory matches experiment for the appropriate degree of truncation. In addition, we perform simulations of a stochastic atomistic-level model incorporating a realistic description of diffusive hopping for under-coordinated surface atoms thereby providing a visualization of the initial reshaping process.

Supporting Information

INTRODUCTION

The ability to synthesize metallic nanocrystals (NCs) with desired shapes and sizes opens the possibility to fine-tune properties for applications such as catalysis or plasmonics.[1,2] However, such nanostructures are intrinsically metastable as there exists a driving force for these systems to evolve back to their equilibrium Wulff shapes.[3,4] Such reshaping, which is generally mediated by surface diffusion, can degrade properties. Thus, thermal shape stability is a fundamental issue. However, comprehensive experimental assessment of reshaping energetics and kinetics, as well as reliable atomistic-level theory and modeling of such phenomena, is currently limited.

Two previous experimental studies of reshaping are particularly instructive in motivating the analysis of this paper. An early in-situ transmission electron microscopy (TEM) analysis[5] indicated that ~8 nm Pt nanocubes reshape at around 500 °C, and pre-melt at above 600 °C. Pt tetrahedra were observed to be somewhat more resistant to

reshaping. It was suggested that there was some degree of edge and corner truncation as the temperature was raised to 350 °C, but that substantial reshaping only occurred at higher temperature. Another study by the same group noted that truncation was common for synthesized Pt nanoclusters, e.g., nanocubes with {100} side facets had truncated corners presenting {111} facets, and truncated edges presenting {110} facets.[6] A more recent TEM analysis[7] explored the thermal stability against reshaping of Pd@Pt_{4L} core-shell NCs, where observed trends at least for the initial stage of reshaping are expected to correspond to those for pure Pt nanocrystals. The onset of observed reshaping for the Pd@Pt_{4L} nanocubes was around 500 °C consistent with the earlier study. Far less facile reshaping was observed for octahedra. These observations prompted DFT analysis[7] which found a low (high) barrier of 0.6 eV (2.0 eV) to extract a 5-fold coordinated (7-fold coordinated) Pt atom from the edge of a complete nanocube (octahedron) to a {100} facet (to a {111} facet).

Our study will consider Pd (rather than Pt) nanocubes, although we will provide an appropriate recipe to relate behavior for different metals. However, for any metal, detailed interpretation and theoretical analysis of NC reshaping should account for two key factors which will be a central component of our analysis. Firstly, sustained reshaping requires not just transport of edge or corner atoms to side facets, but also the nucleation of new layers on those side facets. This nucleation process can control the effective barrier and overall rate for reshaping.[3,8-10] Secondly, as indicated above, synthesized NCs before reshaping will generally exhibit some degree of truncation of edges and corners rather than constituting “complete” cubes or octahedra. We find that the degree of truncation is a key factor in determining reshaping kinetics.

As indicated above, we will consider the reshaping of Pd nanocubes. There exist numerous previous studies reporting the synthesis of these structures.[11-15] An early study which synthesized Pd nanocubes from 8 to 50 nm revealed the presence of a small proportion of {111} facets (i.e., corner truncation) in addition to the dominant {100} side facets.[11] In this and many other studies, the nanocubes are often supported on a {100} face on some substrate, and TEM images provides a birds-eye view looking down on the top {100} facet. Rounding at the corners of the top facet in this view corresponds to truncation of the edges of the nanocube and is typically evident in images. Thus, one expects Pd nanocubes to have both truncated corners and edges, as for Pt nanocubes discussed above. As an aside, we note interest in the growth of concave Pd nanocubes in earlier studies by a seeded approach starting with slightly truncated convex Pd nanocubes,[16,17] and later by a one-pot synthesis approach.[18] However, initial reshaping of concave versus truncated convex nanocubes is fundamentally different (the former being intrinsically more facile),[4] and we do not discuss the concave case further.

In this study, we present results of a comprehensive TEM analysis of the reshaping of Pd nanocubes over a range of temperatures where evolution occurs on an experimentally accessible time scale. This allows extraction for the first time of the effective Arrhenius barrier for the reshaping process. Interpretation of behavior is aided by application of multiple complementary modeling strategies. These include: development of a realistic atomistic-level modeling; analytic determination of the minimum energy path (MEP) for mass transport from {110} edges and {111} corners to {100} side facets of the nanocube, the process which underlies reshaping; coarse-grained continuum analysis of the MEP for reshaping which provides additional insight

into its form; complementary Kinetic Monte Carlo (KMC) simulation of a stochastic model for visualization of mass transport, and validation of the analytic theory.

RESULTS AND DISCUSSION

TEM Analysis of the Reshaping of Pd Nanocubes. Pd nanocubes were synthesized with a mean width between opposite {100} facets (i.e., mean edge length) of 24.1 ± 2.4 nm and a mean diagonal length of 31.3 ± 2.8 nm, as described in the Methods section. To analyze and quantify reshaping, we utilize TEM imaging thereby exploiting rapid advances in this technique which enable direct monitoring of structural and morphological evolution in physicochemical systems at the nanoscale.[19-21] A comprehensive TEM analysis of reshaping was performed at four temperatures (T) in the range T = 410 °C to 440 °C where the high-temperature treatment was carefully controlled *ex situ*. See the Methods section for a more detailed description. Images of nanocube shapes were obtained at multiple times during reshaping at each temperature. These clearly reveal transformation from a cubic to a roughly spherical particle. Our procedure for quantification of the reshaping process is illustrated in **Figure 1** for an approximately 24 nm Pd nanocube at 430 °C. A maximum (d_{max}) and a minimum (d_{min}) caliper length or "diameter" were obtained for the nanocube by considering multiple orientations as shown. We then focused on the time evolution of the ratio $R = d_{max}/d_{min}$. Images showing the corresponding characterization of reshaping at other temperatures are shown in the Supplementary Information (SI).

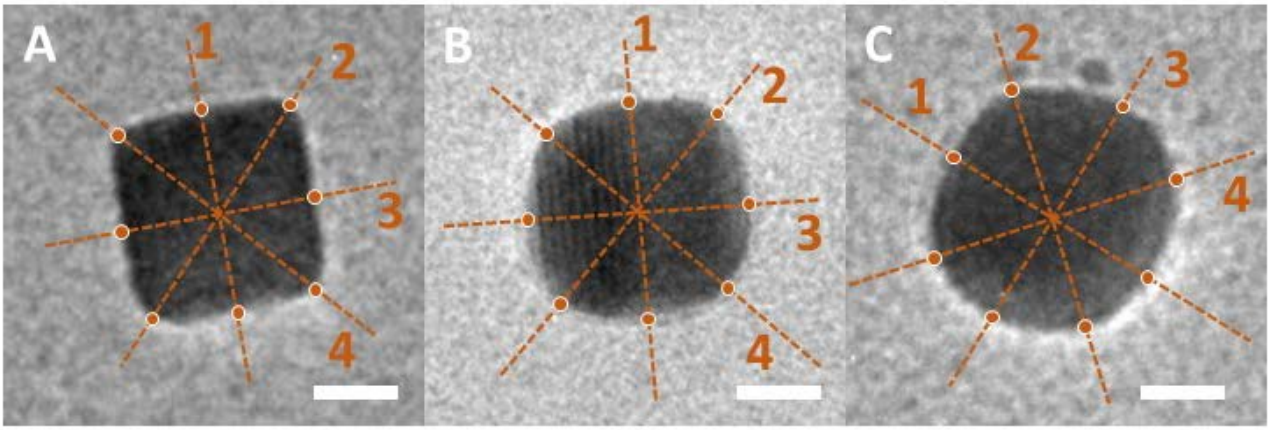

	A (0 min.)	**B** (30 min.)	**C** (90 min.)
d_1 (nm)	24.13	25.38	27.78
d_2 (nm)	30.25	29.18	29.88
d_3 (nm)	23.61	25.94	28.79
d_4 (nm)	30.06	28.51	29.85
d_{max}/d_{min}	1.28	1.15	1.08

Figure 1. Quantification of ~24 nm Pd nanocube reshaping at 430 °C: Synthesized Pd nanocube before heat treatment (A); Pd nanocube from A after 30 min treatment (B); and after 90 min treatment (C). Scale bar: 10 nm.

Figures 2A-2D present TEM images with a larger field-of-view of Pd nanocube reshaping at temperatures T = 410 °C, 420 °C, 430 °C, and 440 °C. Images also indicate the time scale for reshaping with each T. Reshaping behavior is quantified in **Figure 2E** which shows the decrease of the ratio $R(t) = d_{max}/d_{min}$ versus time, t. R generally starts at around $R(0)$ = 1.30 for the synthesized nanocubes and decreases monotonically. The analysis was repeated for 15 different nanocubes at 410 °C and 420 °C, 12 nanocubes at 430 °C and 10 nanocubes at 440 °C, which allowed assessment of uncertainties as indicated by the error bars in **Figure 2E**. We should note that a larger standard deviation for the particles prior to heat treatment (t = 0 min) was because of the different extent of rectangular shape in the nanocubes. During the reshaping process, such asymmetry diminished.

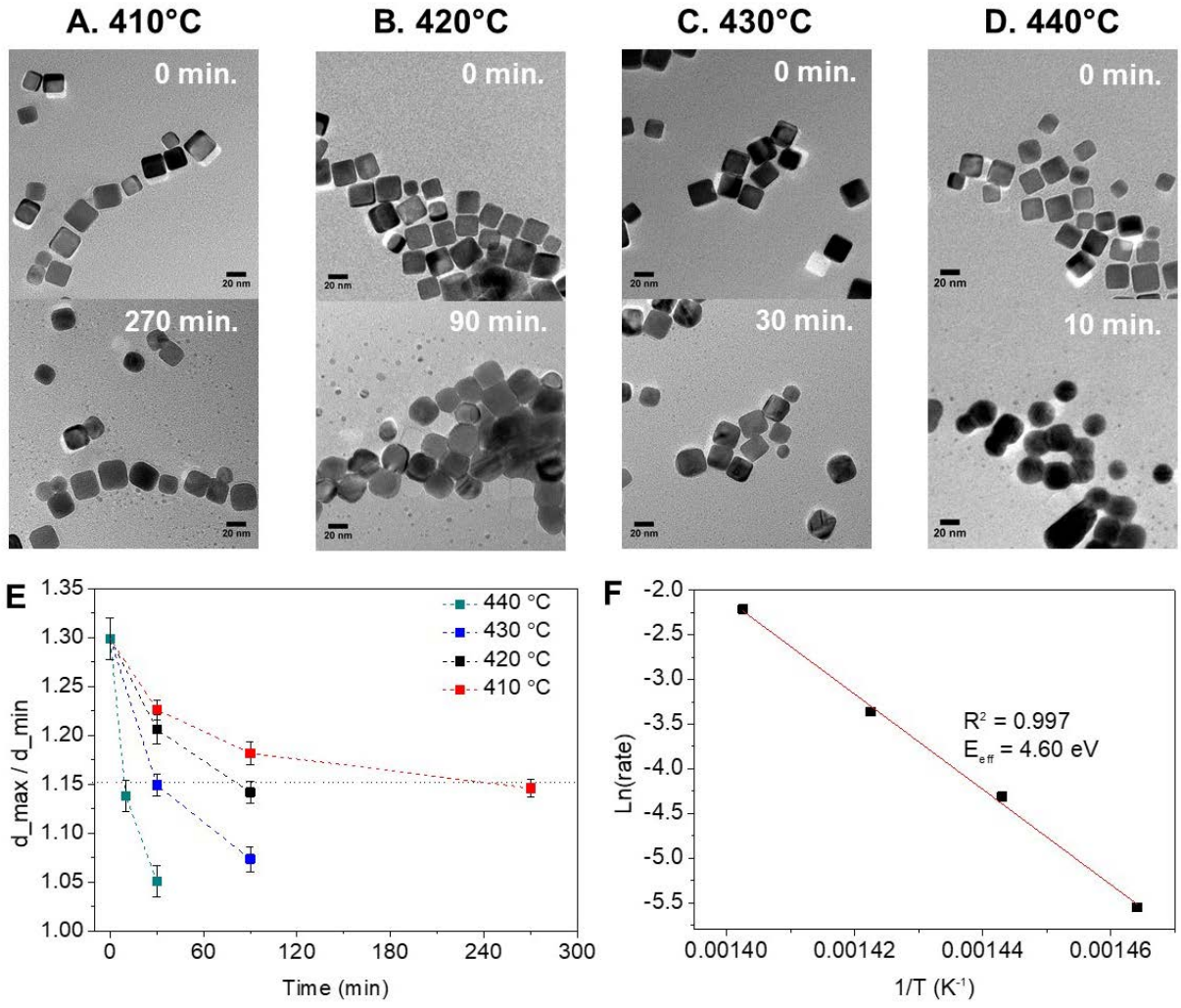

Figure 2. A-D. TEM images of initial synthesized Pd nanocubes, and subsequent reshaped nanocube structures for the temperatures indicated. Scale bar: 20 nm. The times selected for the reshaped structures reflect the characteristic time for reshaping at each temperature. **E**. Ratio $R(t) = d_{max}/d_{min}$ versus time, t for four temperatures. **F**. Arrhenius plot for the reshaping rate $k_{reshape} = 1/t_{char}(T)$ where t_{char} corresponds to R^* = 1.15.

To extract a characteristic time, $t_{char} = t_{char}(T)$, for reshaping at each T, one can choose a threshold value $R^* < R(0)$, and determine t_{char} from $R(t_{char}) = R^*$. The values of t_{char} are of course dependent on the choice of R^*. However, the value of the associated Arrhenius energy, E_{eff}, which is of primary interest, should not depend significantly on R^* (for sufficiently precise data). For our data, the most reliable estimate of E_{eff} should come from choosing R^* around 1.15 (as there is a data point for each T close to this value, and also as a significant time has elapsed even for the highest T making data more reliable). Choosing $R^* = 1.15$, we extract t_{char} for each T by smooth interpolation of the data points. A corresponding Arrhenius plot is presented in **Figure 2F** for the reshaping rate, $k_{reshape} = 1/t_{char}(T) \propto \exp[-E_{eff}/(k_B T)]$, where k_B denotes Boltzmann's constant. This analysis yields $E_{eff}(\text{expt}) \approx 4.60$ eV. Repeating this analysis choosing R* = 1.14, and applying a slight extrapolation of the experimental data for low T, yields $E_{eff}(\text{expt}) \approx 4.74$ eV. (Repeating the analysis for significantly higher $R^* = 1.175$, where there is much more uncertainty in the interpolated t_{char} values, yields $E_{eff}(\text{expt}) \approx 4.09$ eV.) We regard the estimate for $R^* \approx 1.15$ as most reliable, and assign $E_{eff}(\text{expt}) = 4.6 \pm 0.2$ eV. This value is far larger than the barrier for any individual atomic hopping process for crystalline Pd surfaces. The latter claim is confirmed by DFT analysis of the associated barriers. See Ref. 22 and the SI.

Atomistic-level Description of Surface Diffusion Mediated Reshaping. Comprehensive understanding and analysis of the type of reshaping process illustrated above requires an appropriate atomistic-level picture or model of the phenomenon. It is well-recognized that reshaping of metallic nanocrystals is typically mediated by diffusion of under-coordinated atoms across the nanocrystal surface, so our modeling is based upon this mechanism. Given the crystalline fcc structure of the Pd nanocubes, we naturally adopt the framework of stochastic lattice-gas modeling. In such models, all atoms in the nanocrystal reside at the sites of a single-crystal fcc lattice. System thermodynamics can be reliably described by assigning an effective nearest-neighbor (NN) attractive interaction of strength $\phi_{eff} > 0$.[4,23] Model dynamics involves the hopping of under-coordinated surface atoms to neighboring available fcc surface sites. The key model input is a prescription of hopping rates, where these rates depend on the local surface environment and are consistent with system thermodynamics. Evolution of such stochastic models is determined precisely by KMC simulation which implements hops with probabilities proportional to their physical rates. It is significant to note that KMC simulation of these models can capture behavior on the experimentally relevant time scale of minutes to hours for the reshaping phenomena of interest here, in contrast to conventional molecular dynamics simulation.

First, we comment further on system thermodynamics. Although this can be described well by effective NN interactions, we emphasize that ϕ_{eff} must be selected to optimally recover surface thermodynamics and diffusion kinetics <u>not</u> bulk thermodynamics.[4,10] Let a denote the surface lattice constant, so that $a = 0.275$ nm for Pd. Then, ϕ_{eff} can be chosen to match DFT estimates of surface energies[24] using the relations $\gamma_{111} = 3/2\ \phi_{eff}/\Omega_{111}$ for {111} facets with unit cell area $\Omega_{111} = \sqrt{3}a^2/2$, or $\gamma_{100} = 2\phi_{eff}/\Omega_{100}$ for {100} facets with unit cell area $\Omega_{100} = a^2$. This yields $\phi_{eff} \approx 0.36$-0.37 eV for Pd. Our direct DFT analysis of lateral interactions in adsorbed layers on various facets

suggests the assignment of a lower value for $\phi_{eff} \approx 0.29$-0.31 eV for Pd. See Ref. 22 and the SI. Thus, for the current modeling, we select a compromise value of $\phi_{eff} = 0.32$ eV for Pd. If E_c denotes the bulk cohesive energy,[25] then our selected value of ϕ_{eff} is far below the choice $\phi_{bulk} = E_c/6 = 0.65$ eV for Pd which would recover bulk thermodynamics. This prescription of surface thermodynamics, and specifically the value of ϕ_{eff}, will be a key component in determining the effective barrier, E_{eff}, and thus the time scale for reshaping.

Next, we describe in more detail model dynamics. The rates for hopping of under-coordinated surface atoms in various local environments are chosen to have an Arrhenius form, $h = \nu \exp[-E_{act}/(k_B T)]$. Typically, the prefactor is set to $\nu \approx 10^{12.5}$/s, but this choice will not impact our analysis. System thermodynamics is captured through the feature that the activation barriers, E_{act}, must satisfy detailed-balance. Let $E_{i(f)} = n_{i(f)}\, \phi_{eff}$ denote the initial (final) state energy of an atom before (after) hopping, where $n_{i(f)}$ is the coordination. Then, a common prescription of barriers is the bond-counting IVA choice, $E_{act} = E_0 - E_i$, where E_0 is an adjustable parameter.[4,8,9] However, IVA cannot predict the absolute time scale for evolution, and it fails dramatically for fcc metal surfaces to predict correct relative values of terrace and step edge diffusion on a single facet, or of terrace diffusion on different facets.[3,10] Thus, we instead adopt a refined symmetric BEP formulation[3,10] where $E_{act} = E_\alpha + ½\,(E_f - E_i)$. This choice can be tuned to incorporate precise values of barriers obtained from our DFT analysis for different classes, α, of hops. This includes terrace diffusion barriers, $E_d(100) \approx 0.65$ eV for {100} facets and $E_d(111) \approx 0.11$ eV for {111} facets, and edge diffusion barriers $E_e \approx 0.42$-0.45 eV. See the Methods section, and Ref. [3,10], as well as the SI, for details.

Initial Nanocube Truncations. We consider truncations involving both the edges and the corners of nanocubes. It is convenient to label these by the extent of truncation of the edges. Starting from a complete nanocube, the lowest-order truncation, T1, removes a single row of 5-coordinated atoms from each edge. This exposes a double row of 6-coordinated atoms. The second-order truncation, T2, additionally removes this double row of edge atoms to expose a triple row of edge atoms, etc. Thus, the j^{th}-order truncation, Tj, creates a {110} edge facet composed of rows of length $L_e = j + 1$ atoms. Truncation of the edges automatically results in truncation of the corners to expose generally distorted hexagonal {111} facets. Specifically, these six-sided {111} facets have three edges of length L_e as a result of the edge truncation, but the other three edges generally have a different length L_c, which can take values $L_c \geq 3$. See **Figure 3**. Here and below, all lengths are measured in units of atoms.

Our strategy is to choose a reasonable value of L_c for each $L_e = j + 1$ thereby obtaining a single-parameter set of truncations, Tj, for which we analyze reshaping. At this point we note that birds-eye TEM images of nanocubes supported on a {100} facet allow at least estimation of L_e, but not of L_c since corner facets are not generally visible. One might anticipate that a natural "default" choice selects similar L_c and L_e (i.e., $L_e = j+1$ and $L_c = j+2$ for odd j, or $L_c = j+1$ for even j). See **Figure 3** for j = 1 and the SI for j > 1. However, we find that there are issues with this default choice. Significant reshaping requires transfer of atoms from corners and/or edges to nucleate or form new layers on {100} side facets. However, with the above default prescription of Tj, for all but T1, it is energetically far easier to transfer atoms from {111} corner faces to {110} edge

facets rather than to {100} side facets. See the SI. This indicates that the choice of initial structures for the default truncation is artificial in that these would quickly restructure even at much lower T than for which substantial reshaping is observed above 400 °C. Consequently, we chose a modified sequence of truncations Tj where for each L_e = j+1, L_c is chosen sufficiently large that the effective energy barrier to transfer atoms from {111} corners to {100} sides is equal to or smaller than that to transfer atoms from {111} corners to {110} edges. With this prescription, successive truncations T1, T2, T3, etc. are characterized by (L_e, L_c) = (2,3), (3,5), (4,9), etc. See **Figure 3**. A more comprehensive listing is given in **Table 1**.

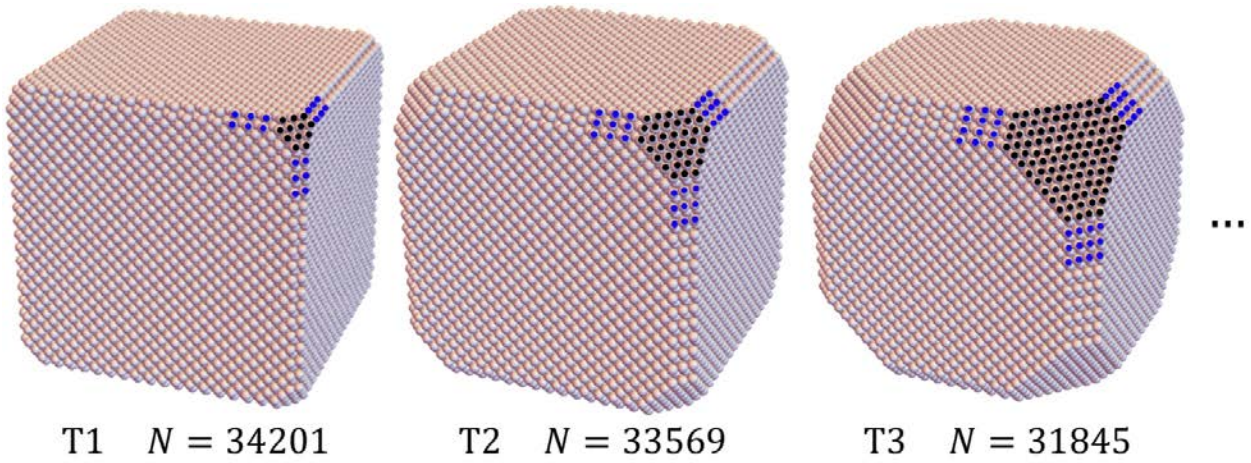

Figure 3. Truncations of nanocubes for T1, T2, and T3 with (L_e, L_c) = (2, 3), (3, 5) and (4, 9), respectively. Surface atoms in a corner {111} facet are indicated by black dots, and edge atoms in {110} facet close to this corner facet are indicated by blue dots.

Table 1. Values of L_e (2nd row), L_c (3rd row), and the maximum energy ΔE_{max} (in units of ϕ_{eff}) along the MEP for mass transfer from edges (e) to sides (4th row), and from corners (c) to sides (5th row) for various truncations Tj of nanocubes.

truncat	T1	T2	T3	T4	T5	T6	T7	T8	T9	T10	T11	T12	T13	T14	T15	T16	T17	T18	T19
Le	2	3	4	5	6	7	8	9	10	11	12	13	14	15	16	17	18	19	20
Lc	3	5	9	11	13	15	19	21	23	27	29	31	33	37	39	41	45	47	49
ΔE_{max}|e	3	4	5	6	7	8	9	10	11	12	13	14	15	16	17	18	19	20	21
ΔE_{max}|c	3	4	6	7	8	9	11	12	13	15	16	17	18	20	21	22	23	25	26

Analytic Determination of the MEP for Reshaping. As noted above, reshaping involves the transfer of atoms from edges and/or corners to create new layers on {100} facets. If one tracks the cumulative energy change, $\Delta E(q)$, subsequent to transfer of the q^{th} atom, then one finds that $\Delta E(q)$ initially increases with q from $\Delta E(0) = 0$, but passes through a maximum, $\Delta E_{max} = \max_q \Delta E(q)$, and subsequently decreases below zero. The initial increase in $\Delta E(q)$ reflects the low initial mean coordination of atoms incorporated in a just-formed small 2D island on a {100} facet (relative to their higher mean coordination on {110} side facets or {111} corner facets). However, as the 2D island grows on the large {100} facet, the mean coordination of incorporated atoms increases above that on the smaller {110} or {111} facets from which they were drawn. This leads

to a decrease below zero in $\Delta E(q)$. The minimum energy pathway (MEP) for reshaping corresponds to a specific sequence for removal of atoms from edges or corners, and a specific sequence of addition to the growing island on the {100} facet, which results in the smallest value of ΔE_{max}. This value of ΔE_{max} is a key factor controlling the effective barrier, E_{eff}, for reshaping.

Some further general comments on the mass transfer process associated with the MEP are appropriate. Initially a new layer is formed on a single {100} side facet, and this grows as a roughly square 2D island, in order to maximize the gain in bonding. If atoms are drawn from edges, then a single layer is removed from each of the 12 edges before removing subsequent layers so as to minimize the increase in system energy during the process. If atoms are drawn from corners, then analogously first a single layer is removed from each of the eight corners, before removing subsequent layers. Our analysis assumes that the nanocluster is sufficiently large that atoms drawn from multiple edges or corners can be incorporated within a compact 2D cluster on a single side facet, i.e., we consider the early stage of reshaping well before a new complete layer on a {100} side facet is formed. Thus, the MEP results below will not depend on NC size, but they do depend strongly on the degree of truncation, and thus on L_e. Note that the above analysis does not incorporate entropic effects. However, comparison with results from KMC simulation of the realistic stochastic model shows that our analysis is effective for the temperature range of interest.

Explicit Evaluation of the MEP for Various Truncations. $\Delta E(q)$ can be decomposed into two components. One component considers the energetics associated with forming a near-square island on a {100} side facet. Let C_q denote the number of bonds formed upon adding the q^{th} atom to this 2D island in such a way as to maximize the number of bonds formed. The other component considers the energetics of removing atoms from {110} edge or {111} corner facets. Suppose that removing the q^{th} atom from one of these facets breaks B_q bonds. Explicit values for C_q and B_q are given in the next subsection. Let the energy change upon transfer of the q^{th} atom be denoted by ΔE_q. Then, the cumulative energy change $\Delta E(q)$ after transfer of the 1^{st}, 2^{nd},…, and q^{th} atom follows from

$$\Delta E(q) = \sum_{1 \le p \le q} \Delta E_p, \text{ where } \Delta E_p = (B_p - C_p)\, \phi_{eff}. \quad (1)$$

Below, we explicitly evaluate $\Delta E(q)$ versus q for various truncations.

First, we quantify energetics associated with forming a near-square island on a {100} side facet. Each atom transferred to the {100} facet forms four bonds to atoms in the supporting {100} layer, and can form additional lateral bonds. Adding the q^{th} atom to this 2D island in such a way to maximize the number of bonds formed creates

$$C_q = 4,5,5,6 \mid 5,6;5,6,6 \mid 5,6,6;5,6,6,6 \mid 5,6,6,6;5,6,6,6,6 \mid,\ldots \text{ bonds for } q = 1,2,\ldots \quad (2)$$

Here, the symbol | indicates completion of square 2D structures, where the pattern for larger q is clear.

Next, we determine the MEP for reshaping corresponding to transfer of atoms from {110} edges to a single {100} side facet. Each atom on the {110} side facet has five bonds to atoms in the supporting {110} layer, and can have additional lateral bonds. Again, truncation Tj corresponds to {110} edge facets with rows of length j+1 atoms.

Removing each atom in a single row breaks 6 bonds, except for removal of the last which breaks only 5 bonds. Thus, one has that B_q = $(6)^j$, 5, $(6)^j$, 5,…, where $(6)^j$ indicates that 6 is repeated j times. Explicit examples of the corresponding ΔE(q) for low-order truncations are now provided. For T1 where B_q = 6,5,6,5…, one finds that

$\Delta E(q)/\phi_{eff}$ = 2,2,3,2,3,2,3,2,2,2,2,1,2,1,1,0,1,0,0,-1,…. for q = 1, 2,… (T1). (3)

This analysis illustrates the general features of $\Delta E(q)$ versus q described above, and reveals that $\Delta E_{max} = 3\phi_{eff}$ for T1. For T2, where B_q = 6,6,5,6,6,5,…, one finds that

$\Delta E(q)/\phi_{eff}$ = 2,3,3,3,4,3,4,4,3,4,4,3,4,4,3,3,4,3,3,3,3,… for q = 1,2,… (T2). (4)

Values do not exceed 4 before decreasing, so that $\Delta E_{max} = 4\phi_{eff}$ for T2. **Figure 4** illustrates the variation of $\Delta E(q)$ with q for {110} edge to {100} side mass transfer for truncations T1 - T20 based on the type of analysis illustrated above for T1 and T2. Corresponding values of ΔE_{max} for T1 - T20 are listed in **Table 1**. Note that the above analysis does not depend on L_c.

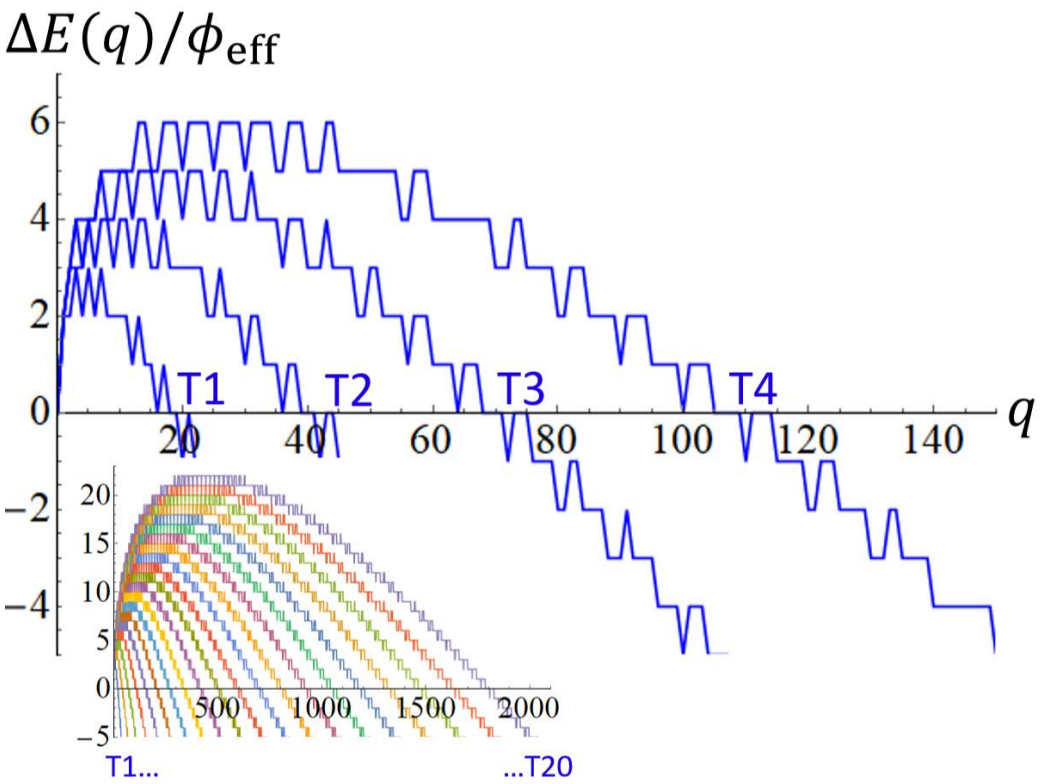

Figure 4. $\Delta E(q)$ vs q for {110} edge to {100} side mass transfer for truncations T1 - T4 (and T1 - T20 in the inset).

Lastly, for transfer of atoms from {111} corners to a single {100} side, we explicitly determine the corresponding B_q and the determination of $\Delta E(q)$ for low-order truncations. For T1, removing atoms from each 12 atom {111} corner facet with (L_e, L_c) = (2, 3) corresponds to a sequence of B_q = 6,5,6,5,5,6,5,5,5,5,4,3 broken bonds for q =

1 - 12, and this sequence is repeated for higher q as atoms a removed from successive corners. Thus, one has $\Delta E(q)/\phi_{eff}$ = 2,2,3,2,2,2,2, 1,0,0,-2,-5,… for q = 1,2,…, again illustrating the general features described above, and that $\Delta E_{max} = 3\phi_{eff}$. For T2, 36 atom {111} corner facets with (L_e, L_c) = (3,5) corresponding to B_q = 6,6,5,6,6,6,5,6,5,… one finds that $\Delta E(q)/\phi_{eff}$ = 2,3,3,3,4,4,4,4,3,… (values not exceeding 4 before decreasing) for q = 1,2,…, so that $\Delta E_{max} = 4\phi_{eff}$. Results for ΔE_{max} from this type of analysis for T1 - T20 are also listed in **Table 1**. Since ΔE_{max} is lower for {110} edge to {100} side mass transfer (except for T1 and T2), we focus on this case as determining the effective barrier for reshaping.

Coarse-grained Continuum Modeling of the MEP. The above atomistic-level modeling provides a precise MEP and ΔE_{max} for each specific truncation. However, additional insight can be provided by coarse-grained (CG) modeling. This CG approach utilizes a continuum framework to analyze the energy change upon transfer of atoms from edges or corners to a square 2D island nucleated on a single {100} side facet. The number of atoms transferred, q, is now regarded as a continuous variable.

In this analysis, the energy associated with the near-square $q = L_{100} \times L_{100}$ atom island on a {100} facet is decomposed into 2D bulk and edge components $\Delta E_{100} = \Delta E_{100}(\text{bulk}) + \Delta E_{100}(\text{edge})$. One has that $\Delta E_{100}(\text{bulk}) = -6\phi_{eff}\, q$, as each atom in the island interior is bonded to 4 atoms in the supporting layer, and has 4 shared lateral bonds. Also, one has that $\Delta E_{100}(\text{edge}) = (\frac{1}{2}\,\phi_{eff})4L_{100}$, as the step energy is $\frac{1}{2}\,\phi_{eff}$ per atom, and $4L_{100}$ is the perimeter length in atoms.

First, considering mass transfer from the {110} edge facets, the energy associated with the removed rows can be written as $\Delta E_{110} = \Delta E_{110}(\text{bulk}) + \Delta E_{110}(\text{edge})$. Here, one has $\Delta E_{110}(\text{bulk}) = -6\phi_{eff}\, q$ (as each atom is bonded to 5 atoms in the supporting layer, and has 2 shared lateral bonds if it is in the row interior). Also, one has that $\Delta E_{100}(\text{edge}) = (\frac{1}{2}\phi_{eff})2(q/L_e)$, as the step energy is $\frac{1}{2}\phi_{eff}$ per atom, q/L_e give the number of rows, and the factor of 2 accounts for two ends of each row.

Consequently, the change in energy upon mass transfer is given by

$$\Delta E(q) = \Delta E_{100} - \Delta E_{110} = \Delta E_{100}(\text{edge}) - \Delta E_{110}(\text{edge}) = [2q^{1/2} - (q/L_e)]\,\phi_{eff}. \qquad (5)$$

This result can be rewritten in naturally rescaled form as $\Delta E = (2u^{1/2} - u)\,\phi_{eff}\, L_e$, where $u = q/(L_e)^2$. This simple analytic form matches well the curves shown in **Figure 4** at least for larger j, as illustrated in **Figure 5** for T20. One determines $\Delta E_{max} = \Delta E(q_{max})$ from the condition that $d/dq\ \Delta E(q) = 0$ for $q = q_{max}$. This analysis yields $q_{max} = (L_e)^2$ or $u_{max} = 1$, and $\Delta E_{max} = \phi_{eff}\, L_e$ capturing well the results in **Table I**. Significantly, our CG analysis simply elucidates the linear increase in ΔE_{max} with truncation order.

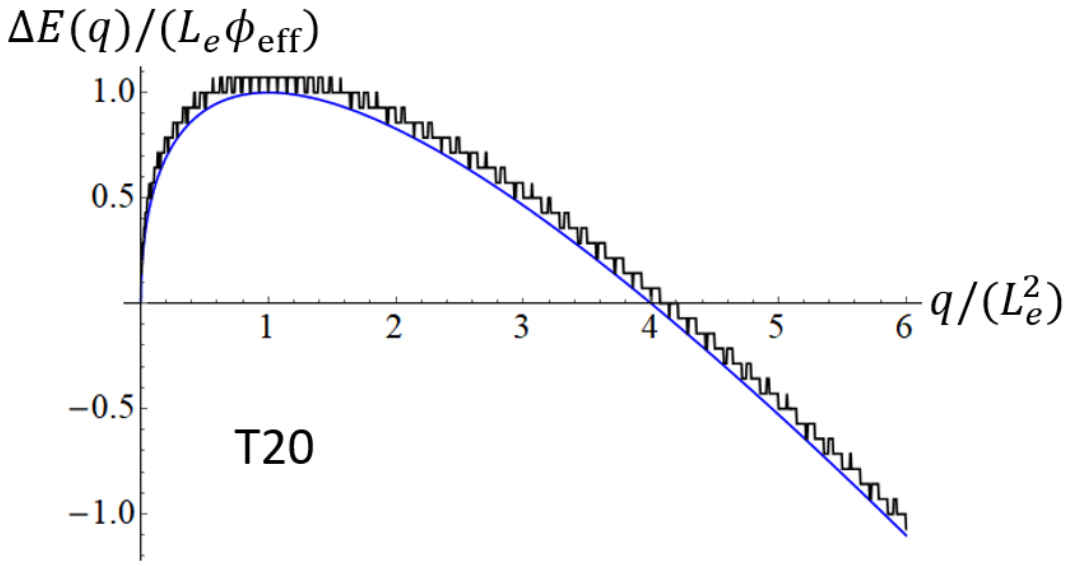

Figure 5. Comparison of results from atomistic-level analysis (black lines) and coarse-grained continuum analysis (blue curve) for $\Delta E(q)$ versus q for truncation T20.

Second, we discuss only briefly transfer from {111} corner facets since mass transfer from edges should typically dominate. This analysis is more complex than that above. For a corner facet with side lengths L_e and L_c ($>L_e$), removal of atoms which minimizes energy cost occurs in two steps. First, atoms are repeatedly removed from the shorter edges of the distorted hexagonal facet until those edges grow and the longer edges shrink to achieve equal length of $(2L_e + L_c)/3$. Subsequently, this hexagonal facet shrinks by continued atom removal, but retains its hexagonal shape. One writes $\Delta E_{111} = \Delta E_{111}(\text{bulk}) + \Delta E_{111}(\text{edge})$ for the energy associated with the removed atoms with $\Delta E_{111}(\text{bulk}) = -6\phi_{\text{eff}}\, q$, as each atom is bonded to 3 atoms in the supporting layer and has 6 shared lateral bonds in the island interior. Thus, $\Delta E(q) = \Delta E_{100}(\text{edge}) - \Delta E_{111}(\text{edge})$ follows from determination of $\Delta E_{111}(\text{edge})$ which measures step energy changes associated with the shrinking edge length. Continuum predictions again match well a discrete atomistic analysis. See the SI.

KMC Simulation of {100} Layer Formation on Pd nanocubes. KMC simulation of the realistic stochastic model for Pd nanocube reshaping described above (see the Methods section) can be used to visualize the process of reshaping, and specifically the formation of new layers on {100} facets. In addition, KMC simulation can assess the effective barrier for reshaping, E_{eff}, which has the form $E_{\text{eff}} = E_{\text{diff}} + \Delta E_{\text{max}}$. Here, E_{diff} is an appropriate activation barrier for diffusion of atoms being transferred from {110} edges to a {100} side facet. Thus, KMC simulation provides a check on the predictions of analytic theory for ΔE_{max} as a function of the degree of truncation.

However, it is not computationally viable to simulate nanocubes in the experimental size range of ~25 nm, or to simulate higher-order truncations. This is in part due to the feature that we must run 25-50 simulation trials for each parameter choice to accurately capture average behavior given large fluctuations between trials, and allow reliable extraction of E_{eff}. (However, for the T4 truncation at the highest T, we run fewer trials due to computational cost.) Thus, we perform simulations for various

truncated Pd nanocubes with a smaller initial width between {100} facets of just above 8 nm. The nanocube size in atoms will be denoted by N. There are various ways to quantify reshaping including monitoring evolution of the total system energy,[10] or the width between populated {100} layers on opposite sides of the nanocube.[10] Here, instead we track the time, τ_{nuc}, for formation of the first new 2D island on a {100} facet which reaches a prescribed threshold size, N^*. This size is generally chosen so that $\Delta E(q)$ has already achieved its maximum value for $q \leq N^*$.

Specifically, simulations of reshaping were performed for truncations T1-T4 where N = 34201, 33569, 31845, and 29661 atoms, respectively, over a range of temperatures. Arrhenius analysis of the mean time to form a 2D island on a {100} of size N^* = 9 (a 3×3 island) as shown in **Figure 6** determines the effective energy, E_{eff}, for reshaping. For T1, analysis of the variation of τ_{nuc} over roughly 330-530 °C yields E_{eff} = 1.27 eV. Similar analysis yields E_{eff} = 1.90 eV, 2.27 eV, and 2.67 eV for T2, T3, and T4, respectively, but with a higher temperature range (to facilitate simulation of the slower reshaping process for higher-order truncations). These results showing a steady increase of $E_{eff} = E_{diff} + \Delta E_{max}$ with truncation order consistent with theoretical predictions of an increase in ΔE_{max}. They correspond to choosing E_{diff} in the expected range 0.3-0.75 eV, as discussed further in the next subsection. We have repeated analysis for T4 with N^* = 25 (a 5×5 island) since $q = N^* = 9$ is too small for $\Delta E(q)$ to have achieved its maximum, and as expected we obtain a somewhat higher E_{eff} = 2.99 eV.

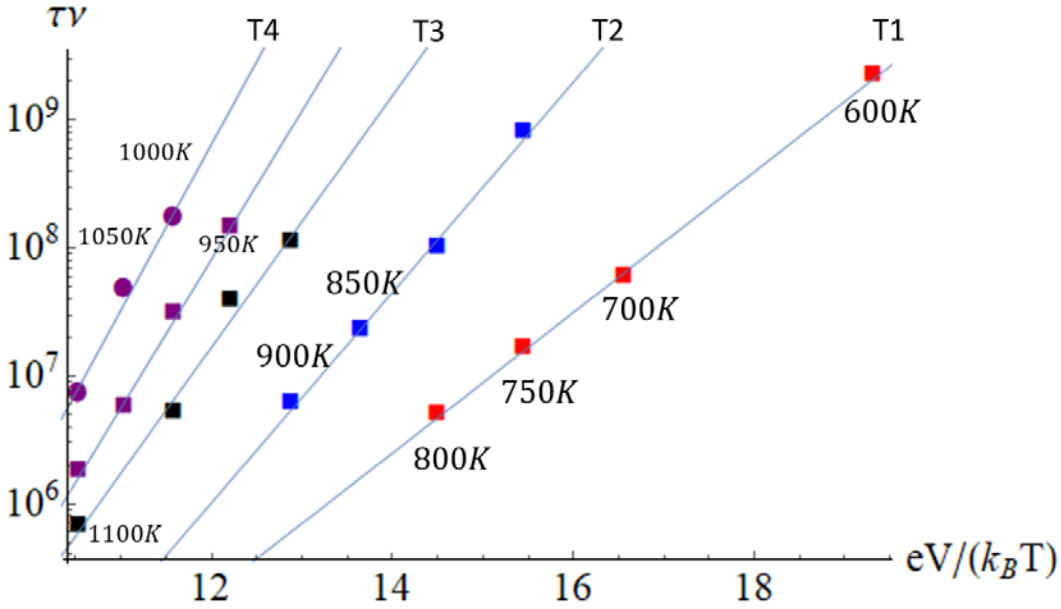

Figure 6. Arrhenius analysis of KMC simulation data for the reshaping time for truncations T1 - T4 for N^* = 3x3 (square symbols). For T4, results are also shown for N^* = 5x5 (circular symbols).

Images of simulated configurations for the initial stage of reshaping are shown in **Figure 7** which provide examples of the first 2D island formed on a {100} facet exceeding the threshold size N^* = 9. Red atoms indicate atoms in locations not

populated in the initial configuration (so, in particular, the just-formed 2D island is indicated by red atoms). Grey atoms show empty sites which were initially populated. The examples shown are typical in that the 2D island is often formed near the periphery of the {100} facet, but one can find examples where it is formed closer to the facet center.

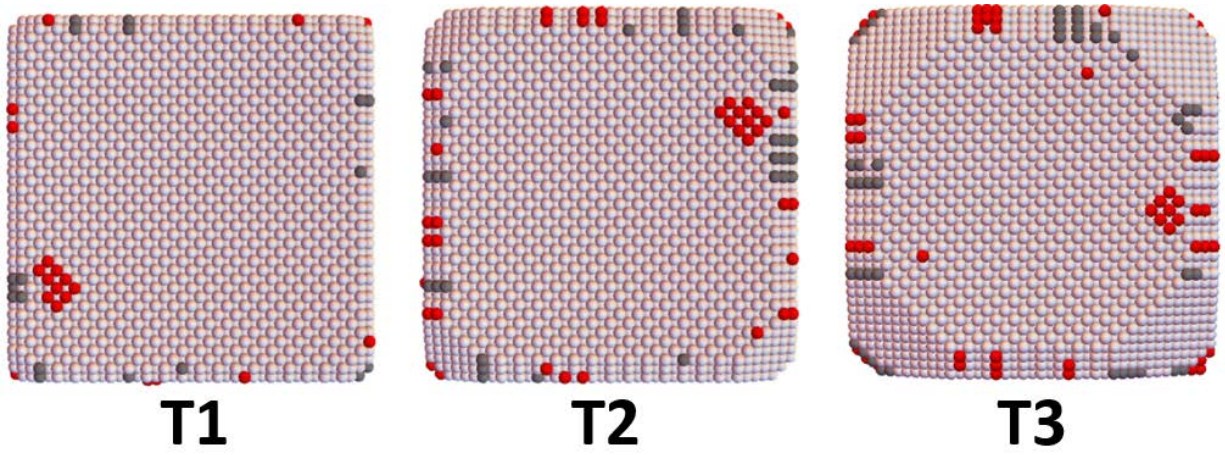

Figure 7. KMC simulations showing a birds-eye view looking down on the {100} facet on which the first 2D island has formed for truncations T1-T3. Red atoms indicate populated sites which were vacant in the initial configuration. Grey atoms represent initially populated sites which are vacant at the later time.

Theoretical interpretation of Experimental TEM results for Pd nanocubes. From our theoretical analysis, the extent of truncation is a critical factor in determining the energetics of reshaping. Examination of multiple TEM images such as **Figure 1** indicate that the width of the {110} edge facet is somewhat above 3 nm (with considerable uncertainty), corresponding to rows of $L_e \approx$ 11-12 atoms. This in turn corresponds to truncations around T10 - T11 with $\Delta E_{max} = 12\phi_{eff} - 13\phi_{eff} = 3.8 - 4.2$ eV for Pd. Thus, the effective barrier for reshaping, $E_{eff} = E_{diff} + \Delta E_{max}$, should be somewhat higher depending on the appropriate value E_{diff} of the barrier for diffusion of atoms from {110} edges to a {100} side facet. If a 2D island on the {100} facet is formed away from the edge of the {100} facet, then E_{diff} should correspond to the terrace diffusion barrier across {100} facets, $E_d(100) \approx 0.65$ eV from DFT (where we assume there is no significant additional Ehrlich-Schwoebel barrier to cross the edge between {110} and {100} facets). Then, our theory would imply that $E_{eff} \approx 4.45 - 4.85$ eV fully consistent with the experimental value of $E_{eff}(expt) \approx 4.6$ eV. It is possible that the 2D island is formed near the edge of the {100} facet (as suggested by simulations reported above) in which case E_{diff} could be lower than $E_d(100)$ (as appears to be the case for KMC simulation for truncation T1).

The key observation from comparison of theory and experiment is that the primary contribution to the observed large $E_{eff}(expt) \approx 4.6$ eV comes from the thermodynamic factor ΔE_{max} associated with the maximum $\Delta E(q)$ along the MEP. It is the feature that this quantity increases quasi-linearly with the degree of truncation which leads to the large value of E_{eff} observed in experiment given substantial truncation of edges and corners in the initial experimental nanocube configuration.

Nanocube Reshaping for Other fcc Metals. The above analytic formulation of the MEP and effective barrier for reshaping, $\Delta E_{max} = m\ \phi_{eff}$ where m = 2, 3, 4,… for T1, T2, T3,… respectively (see **Table 1**), applies for any fcc metal after incorporating the appropriate ϕ_{eff}. E_{eff} is obtained by adding an additional kinetic contribution, E_{diff}, which should roughly scale like ϕ_{eff}. But even if the latter scaling is not well-satisfied, since ΔE_{max} dominates E_{diff} for relevant higher-order truncations, it follows that E_{diff} is roughly proportional to ϕ_{eff}. As a result, the characteristic temperature (in Kelvin) for the on-set of reshaping, $T_{reshape}$, is also roughly proportional to ϕ_{eff}. In **Table 2**, we determine ϕ_{eff} based on DFT values of surface energies for {111} facets ($\phi_{eff} = \phi_{111}$), and also for {100} facets ($\phi_{eff} = \phi_{100}$), assuming that these are controlled by effective nearest-neighbor interactions. Again, we emphasize that these values are far below those (denoted by ϕ_{bulk}) extracted from the bulk cohesive energy. Then, selecting $T_{reshape}$ = 420 °C for Pd, we predict $T_{reshape}$ for other fcc metals for which nanocubes have been synthesized. Using $\phi_{eff} = \phi_{111}$, one obtains $T_{reshape} \approx$ 500 °C for Pt, consistent with experimental observations.[5,7] Au has the lowest and Rh the highest $T_{reshape}$ amongst the metals considered. Using $\phi_{eff} = \phi_{100}$ yields somewhat different values for $T_{reshape}$, but trends between different metals are preserved.

Table 2. Parameters for various fcc metals: (i) the bulk cohesive energy E_c, and corresponding effective bulk nearest-neighbor interaction ϕ_{bulk}; and (ii) the surface energies γ, unit cell areas Ω, associated effective nearest-neighbor interactions, ϕ_{eff}, and corresponding reshaping temperatures $T_{reshape}$ (with values for both {111} and {100} facets).

	Au	**Ag**	**Cu**	**Pd**	**Pt**	**Rh**
E_c (eV/atom)25	3.81	2.95	3.49	**3.89**	5.84	5.75
$\phi_{bulk} = E_c/6$ (eV)	0.64	0.49	0.58	**0.65**	0.97	0.96
γ_{111} (eV/Å^2)^{t24}	0.044	0.048	0.084	**0.085**	0.093	0.124
Ω_{111} (Å^2)	7.21	7.24	5.64	**6.55**	6.65	6.25
$\phi_{111} = 2/3\ \gamma_{111}\,\Omega_{111}$ (eV)	0.21	0.23	0.32	**0.37**	0.41	0.52
$T_{reshape}$ from γ_{111} (° C)	**120**	**160**	**320**	**420**	**500**	**695**
γ_{100} (eV/Å^2)^{t24}	0.054	0.051	0.092	**0.095**	0.116	0.147
Ω_{100} (Å^2)25	8.32	8.36	6.52	**7.57**	7.68	7.22
$\phi_{100} = ½\ \gamma_{100}\,\Omega_{100}$ (eV)	0.23	0.21	0.30	**0.36**	0.45	0.53
$T_{reshape}$ from γ_{100} (° C)	205	215	355	**420**	595	745

CONCLUSIONS

A comprehensive analysis is provided of the reshaping of truncated Pd nanocubes extracting from TEM studies an effective Arrhenius energy $E_{eff} \approx$ 4.6 eV for the process. We show that this large value is not associated with a single atomistic surface diffusion process. Rather, it is controlled by the maximum energy, ΔE_{max}, along the MEP for formation of new layers on {100} facets by transfer of atoms from edges and corners of the truncated nanocube. Of particular significance is the recognition that ΔE_{max} and thus E_{eff} depends strongly on and increases roughly linearly with the extent of truncation of the initial nanocube. Agreement between analytic theory incorporating DFT energetics

and experiment supports the validity of the above picture. KMC simulation of a stochastic atomistic model for reshaping provides a visualization of the key process of forming new layers on {100} facets, and also provides additional support for the analytic theory.

Previous theoretical studies have examined the nucleation-mediated reshaping of convex faceted nanoclusters,[3,4,26] and the long-range diffusion of epitaxially supported faceted nanoclusters,[27] where entire layers are dissolved and reformed on different sides. These studies revealed an increase without bound in effective barrier for reshaping or diffusion with increasing nanocluster size. However, the current analysis of the reshaping of nanocubes is fundamentally different in that the initial kinetics of reshaping depends primarily on the extent of truncation rather than on the overall nanocube size.

We emphasize that the multi-faceted theory and modeling approach introduced in this paper is applicable to any fcc metal. This is illustrated by our prediction of the nanocube reshaping temperatures for various metals for which nanocubes have been synthesized. It should also be noted that our theoretical approach to analyze reshaping can be extended to other nanocrystal shapes such as tetrahedra and octahedra. In fact, application of our approach to analyze MEP reveals that ΔE_{max} is intrinsically higher for octahedra than nanocubes for a similar degree of truncation. This observation, together with the feature that the ends of synthesized octahedra are generally heavily truncated, is consistent with the observed less facile reshaping of octahedra relative to nanocubes.[7]

METHODS

Synthesis of ~25 nm Pd Nanocubes. A vial containing CTAB (0.05 g) and 9.300 mL of deionized water was sonicated until the CTAB was completely dissolved. Pd precursor (0.500 mL of 0.01 M H_2PdCl_4) was added to the solution, and a bright orange color was produced indicating the formation of the precursor complex with CTAB. The solution was then mixed, and 0.200 mL of 0.1 M NaI was added to the solution. The modification to the procedure improves the yield and uniformity of cubes. A color change from bright-orange to a dark-red color was observed after iodide addition. The solution was then heated for 5 min at 95 °C with gentle stirring, after which 0.200 mL of 0.04 M ascorbic acid was added to the vial. The solution was left to heat for an additional 30 min at 95 °C with stirring until the dark red color was completely replaced by a dark-brown color, which indicated the completed formation of the NC substrates. The solution was removed from heat, allowed to cool, and then transferred to a 50 mL centrifuge tube and centrifuged for 15 min at 8000 rpm. The clear supernatant was decanted and discarded to yield a concentrated solution of Pd nanocubes. Seven reactions were repeated in the same fashion for a total of eight reaction solutions. The precipitated fractions were combined and re-dispersed with deionized water to a final volume of 10 mL resulting in a dark-brown colored solution (~4 mM in Pd), which was stored at room temperature for future use. See Ref. 28 for more details.

TEM Analysis of Pd Nanocube Reshaping. TEM observation of Pd nanocube reshaping was performed on a TECNAI G2 F20 electron microscope, under an

accelerating voltage of 200 kV. TEM samples were made with a drop-cast method using Au/SiO_x grids (SPI supplies) to enable heat treatment. Elevated temperature annealing was performed *ex situ* using a Thermo Scientific Lindberg Blue M tube furnace. A quartz tube was allowed to preheat to the target temperature (410-440 °C) with Ar flow at 100 mL/min before the Au/SiO_x grid containing the sample was inserted quickly into the tube. Subsequently at a desired amount of annealing time, the quartz tube was quickly quenched to room temperature with cold water.

DFT Analysis for Pd Surface Energetics. The plane-wave DFT VASP code with the PBE functional was used to determine diffusion barriers for Pd adatoms on both Pd(100) and Pd(111) surfaces including close-packed steps. For the determination of these barriers, we use a 3-layer thick slab including a 1-layer thick strip on one side presenting close-packed steps. (For the determination of ϕ_{eff} for Pd(100), a thicker slab was used to mitigate quantum size effects which are stronger for {100} than {111} orientations.) The vacuum thickness between slab replicas is ~2.2 nm. A $1\times8\times1$ k-mesh is used and an energy cut-off of 250.9 eV. For the Pd(100) surface, we use a 10×6 lateral supercell and the 1-layer strip includes 5×6 atoms. A previous study for this surface used both PBE and PBEsol functionals.[22] For the Pd(111) surface, we use a 20×5 lateral supercell and the 1-layer thick strip includes 10×5 strip atoms, opposite sides of which present A- and B-type steps. To determine minimum energy paths for diffusion, and thus precise activation barriers, the nudged elastic band method is employed. See the SI for details.

KMC Simulation of the Stochastic Atomistic-level Model. As described above, the stochastic lattice-gas model describes reshaping of fcc nanocrystals mediated by surface diffusion with specified rates for hopping of under-coordinated surface atoms to neighboring unoccupied fcc surface sites. There are numerous distinct rates for hopping depending on the local environment of the surface atom, and a key component of our model is realistic prescription of these rates. In each KMC step, an allowed hop (labeled by k) of one atom to a specific neighboring site is implemented with a probability given by the physical rate, h_k, for that hop divided by the total rate for all possible hops, $H = \sum_k h_k$. Physical time during this KMC step is incremented by an amount $\delta t = -\ln(x)/H$ where x is a random number uniformly distributed on [0,1].

ASSOCIATED CONTENT

Supporting Information

The Supporting Information is available free of charge on the ACS Publications website at DOI: 10/1021/acsnano.xxxxxxx.

AUTHOR INFORMATION

Corresponding Author

*E-mail: jevans@ameslab.gov

ORCID

King C. Lai: 0000-0003-2764-356X
Minda Chen: 0000-0002-9881-9350

Yong Han: 0000-0001-5404-0911
Wenyu Huang: 0000-0003-2327-7259
James W. Evans: 0000-0002-5806-3720

Author Contributions

KCL, YH, and JWE performed the DFT analysis and KMC simulation, and developed the analytic theory. MC and WH performed the TEM analysis. BW and CKT synthesized the Pd nanocubes.

Notes

The authors declare no competing financial interests.

ACKNOWLEDGEMENTS

K.C.L, Y.H. and J.W.E were supported for the theoretical analysis (DFT, KMC, and analytic theory) by the US Department of Energy, Office of Science, Basic Energy Sciences, Division of Chemical, Sciences, Geosciences, and Biological Sciences, and their work was performed at Ames Laboratory which is operated by Iowa State University under contract No. DE-AC02-07CH11338. Use of resources from NERSC, a USDOE Office of Science User Facility operated under contract No. DE-AC02-05CH11231, and partly from XSEDE operated under NSF grant ACI-1548562, is also acknowledged. M.C., B.P.W., C.-K.T. and W. H. were partially supported by NSF Grant CHE-1566445.

REFERENCES

(1) Xia, Y.; Xiong, Y.; Lim, B.; Skrabalak, S. E. Shape-controlled Synthesis of Metal Nanocrystals: Simple Chemistry meets Complex Physics? *Angew. Chem. Int. Ed.* **2009**, *48*, 60-103.
(2) Zaera, F. Shape-controlled Nanostructures in Heterogeneous Catalysis. *ChemSusChem* **2013**, *6*, 1797-1820.
(3) Combe, N.; Jensen, P.; Pimpinelli, A. Changing Shapes in the Nanoworld. *Phys. Rev. Lett.* **2000**, *85*, 110-113.
(4) Lai, K. C.; Han, Y.; Spurgeon, P.; Huang, W.; Thiel, P. A.; Liu, D.-J.; Evans, J. W. Reshaping, Intermixing, and Coarsening of Metallic Nanocrystals: Non-equilibrium Statistical Mechanical and Coarse-Grained Modeling. *Chem. Rev.* **2019**, *119*, 6670-6768.
(5) Wang, Z. L.; Petroski, J. M.; Green, T. C.; El-Sayed, M. A. Shape Transformation and Surface Melting of Cubic and Tetrahedral Platinum Nanocrystals. *J. Phys. Chem. B* **1998**, *102*, 6145-6151.
(6) Wang, Z. L.; Ahmad, T. S.; El-Sayed, M. A. Steps, Ledges and Kinks on the Surfaces of Platinum Nanoparticles of Different Shapes. *Surf. Sci*. **1997**, *380*, 302-301.
(7) Vara, M.; Roling, L. T.; Wang, X.; Elnabawy, A. O.; Hood, Z. D.; Chi, M.; Mavrikakis, M.; Xia, Y. Understanding the Thermal Stability of Palladium−Platinum Core−Shell Nanocrystals by In Situ Transmission Electron Microscopy and Density Functional Theory. *ACS Nano* **2017**, *11*, 4571−4581.
(8) Lim, T. H.; McCarthy, D. N.; Hendy, S. C.; Stevens, K. J.; Brown, S. A.; Tilley, R. D. Real-time TEM and Kinetic Monte Carlo Studies of the Coalescence of Decahedral Gold Nanoparticles. *ACS Nano* **2009**, *3*, 3809-3813.

(9) McCarthy, D. N.; Brown, S. A. Evolution of Neck Radius and Relaxation of Coalescing Nanoparticles. *Phys. Rev. B* **2009**, *80*, 064107.
(10) Lai, K.C.; Evans, J.W. Reshaping, Pinch-off and Sintering of 3D fcc metal Nanoclusters: Stochastic Atomistic Modeling with a Realistic Surface Diffusion Kinetics. *Phys. Rev. Materials* **2019**, *3*, 026001.
(11) Xiong, Y.; Chen, J.; Wiley, B.; Xia, Y.; Yin, Y.; Li, Z.-Y. Size-Dependence of Surface Plasmon Resonance and Oxidation for Pd Nanocubes Synthesized via a Seed Etching Process. *Nano Letters* **2005**, *5*, 1237-1242.
(12) Chang, G.; Oyama, M.; Hirao, K. Facile Synthesis of Monodisperse Palladium Nanocubes and the Characteristics of Self-assembly. *Acta Mat*. **2007**, *55*, 3455-3456.
(13) Zhang, H.; Jin, M.; Xiong, Y.; Lim, B.; Xia, Y. Shape-controlled Synthesis of Pd Nanocrystals and their Catalytic Applications. *Acc. Chem. Res*. **2012**, *46*, 1783-1794.
(14) Ding, H.; Dong, J. Synthesis of Palladium Nanocubes/Nanorods and Their Catalytic Activity for Heck Reaction of Iodobenzene. *Appl. Microscopy* **2016**, *46*, 105-109.
(15) Pekkari, A.; Zafer Say, Z.; Susarrey-Arce, A.; Langhammer, C.; Härelind, H.; Sebastian, V.; Moth-Poulsen, K. Continuous Microfluidic Synthesis of Pd Nanocubes and PdPt Core–Shell Nanoparticles and Their Catalysis of NO2 Reduction. *ACS Appl. Mat. Int*. **2019**, *11*, 36196-36204.
(16) Xia, X.; Xie, S.; Liu, M.; Peng, H.-C.; Lu, N.; Wang, J.; Kim, M. J.; Xia, Y. On the Role of Surface Diffusion in Determining the Shape or Morphology of Noble-metal Nanocrystals. *Proc. Nat. Acad. Sci*. **2013**, *110*, 6669-6673.
(17) Xie, X.; Gao, G.; Pan, Z.; Wang, T.; Meng, X.; Cai, L. Large-Scale Synthesis of Palladium Concave Nanocubes with High-Index Facets for Sustainable Enhanced Catalytic Performance. *Sci. Reports* **2015**, *5*, 8515-8519.
(18) Vara, M.; Xia, Y. Facile Synthesis of Pd Concave Nanocubes: From Kinetics to Mechanistic Understanding and Rationally Designed Protocol. *Nano Research* **2018**, *11*, 3122-3131.
(19) Min Yuk, J. M.; Jeong, M.; Kim, S. Y.; Seo, H. K.; Kim, J.; Lee, J. L.
In situ Atomic Imaging of Coalescence of Au Nanoparticles on Graphene: Rotation and Grain Boundary Migration. *Chem. Comm*. **2013**, *49*, 11479-11481.
(20) In-situ Liquid Cell Transmission Electron Microscopy Investigation on Oriented Attachment of Gold Nanoparticles, Zhu, C.; Liang, S.; Song, E.; Zhou, Y.; Wang, W.; Shan, F.; Shi, Y.; Hao, C.; Yin, K.; Zhang, T.; Liu, J.; Zheng; H.; Sun, L. *Nat. Comm*. **2018**, *9*, 421
(21) Ma, T.; Wang, S.; Chen, M.; Maligal-Ganesh, R. V.; Wang, L.-L.; Johnson, D. D.; Kramer, M. J.; Huang, W.; Zhou, L., Toward Phase and Catalysis Control: Tracking the Formation of Intermetallic Nanoparticles at Atomic Scale, *Chem*. **2019**, *5*, 1235-1247.
(22) Han, Y.; Stoldt, C. R.; Thiel, P. A.; Evans, J. W. Ab Initio Thermodynamics and Kinetics for Coalescence of Two-Dimensional Nanoislands and Nanopits on Metal (100) Surfaces. *J. Phys. Chem. C* **2016**, *120*, 21617-21630.
(23) Roling, L. T.; Li, L.; Abild-Pedersen, F. Configurational Energies of Nanoparticles Based on Metal−Metal Coordination. *J. Phys. Chem. C* **2017**, *121*, 23002-23010.
(24) Tran, R.; Xu, Z.; Radhakrishnan, B.; Winston, D.; Sun, W.; Persson, K. A.; Ong, S. P. Surface Energies of Elemental Crystals. *Sci. Data* **2016**, *3*, 160080.
(25) C. Kittel. Introduction to Solid State Physics (Wiley & Sons, New York,1976), 5th Ed.
(26) Mullins, W.W.; Rohrer, G.S. Nucleation Barrier for Volume-conserving Shape Changes of Faceted Crystals. *J. Am. Ceram. Soc.* **2000**, *83*, 214-216.
(27) Lai, K. C.; Evans, J. W. Complex Oscillatory Decrease with Size in Diffusivity of (100)-Epitaxially Supported 3D fcc Nanoclusters. *Nanoscale*, **2019**, *11*, 17506-17516.
(28) Sneed, B. T. Kuo, C.-H. Brodsky, C. N.; Tsung, C.-K. Iodide-Mediated Control of Rhodium Epitaxial Growth on Well-Defined Noble Metal Nanocrystals: Synthesis, Characterization, and Structure-Dependent Catalytic Properties. *J. Am. Chem. Soc.*, **2012**, *134*, 18417-18426.

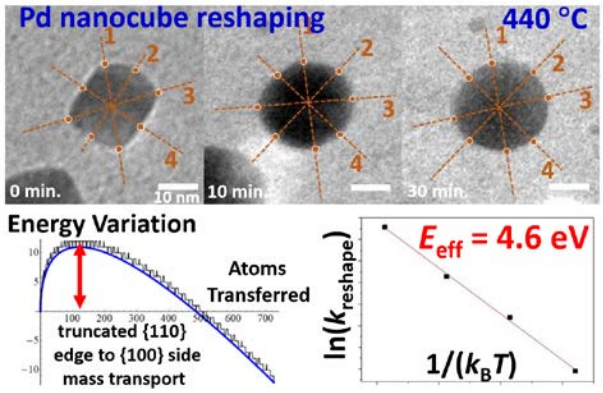

For Table of Contents only